Supporting information for:

Thermal Phase Behavior and Ion Hopping in 1,2,4-Triazolium Perfluorobutanesulfonate Protic Organic Ionic Plastic Crystal

Anirban Mondal,[†] Anurag Prakash Sunda,[‡] and Sundaram Balasubramanian[*,†]

Chemistry and Physics of Materials Unit, Jawaharlal Nehru Centre for Advanced Scientific Research, Bangalore 560064, INDIA, and Materials Research Laboratory, Department of Chemistry, Central University of Haryana, Mahendergarh, Haryana 123029, INDIA

E-mail: bala@jncasr.ac.in

Phone: +91 (80) 2208 2808. Fax: +91 (80) 2208 2766

---

[*] To whom correspondence should be addressed

[†] Chemistry and Physics of Materials Unit, Jawaharlal Nehru Centre for Advanced Scientific Research, Bangalore 560064, INDIA

[‡] Materials Research Laboratory, Department of Chemistry, Central University of Haryana, Mahendergarh, Haryana 123029, INDIA

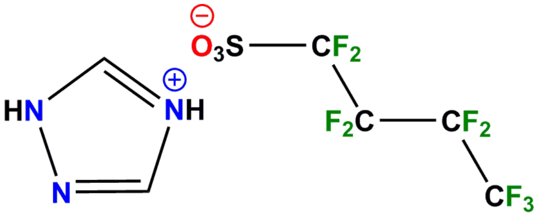

Figure S1: The chemical structure of [TAZ][pfBu] POIPC.

Charge calculation: The atomic site charges were assigned based on DDEC/c3 method.[S1,S2] A 1x1x1 unit cell of the crystal structure determined by experiments[S3] was used to calculate atomic site charges. Density functional theory (DFT) calculations were performed using CP2K[S4] program to optimize the electronic wave functions with a convergence criterion of 10^{-7} on its gradient. Cube files were generated to store the valence electron density and this density information was used as input to the DDEC/c3 program[S1,S2] to obtain atomic site charges. Other details about this charge calculation can be found elsewhere.[S5]

Table S1: Summary of the cell parameters and supercell dimension for the perfect crystal and vacancy model simulations.

System	Cell parameter						Supercell	No. of ion pairs	No. of atoms
	a(Å)	b(Å)	c(Å)	α(^{o})	β (^{o})	γ (^{o})			
Perfect Crystal	5.27	8.27	29.67	90.00	93.12	90.00	(6x4x1)	96	2496
Vacancy Model	5.27	8.27	29.67	90.00	93.12	90.00	(8x6x2)	383	9958

Table S2: Simulated cell parameters and compared against the experimental data at 100 K. Uncertainty in simulated values were of the order of 0.002.

Supercell		a (Å)	b (Å)	c (Å)	α (^{o})	β (^{o})	γ (^{o})	ρ (g/cm^3)
(6x4x1)	exp.	31.645	33.087	29.673	90.0	93.124	90.0	1.897
	sim.	31.877	33.238	29.886	89.73	92.657	89.87	1.899

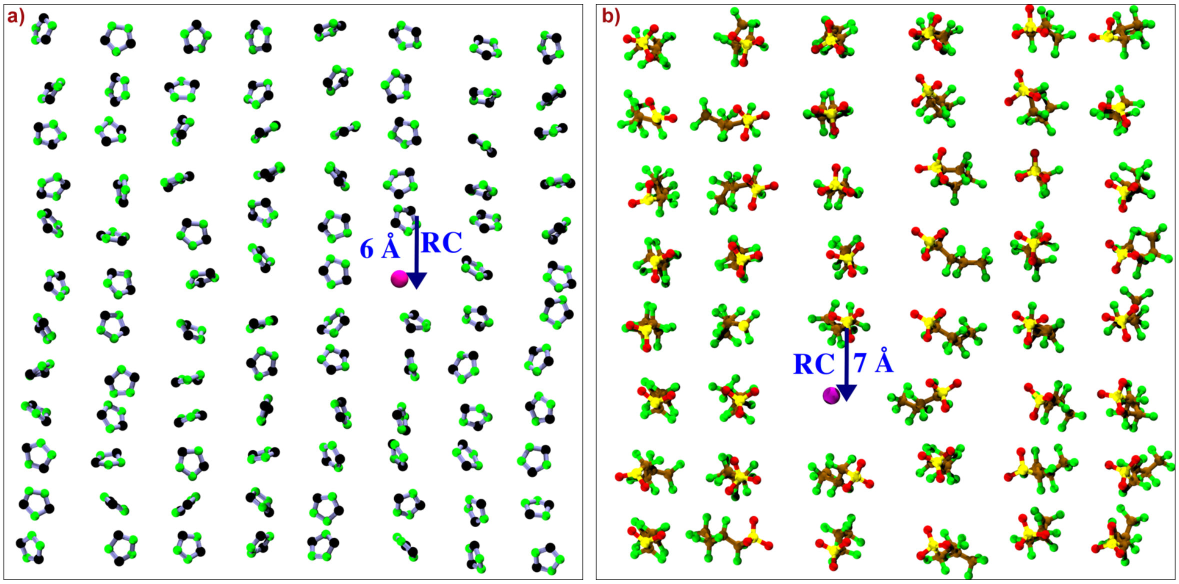

Figure S2: Snapshots show the reaction coordinate (RC) which is defined as the distance between the center of mass of dummy atom and center of mass of the a) cation, and/or b) anion respectively.

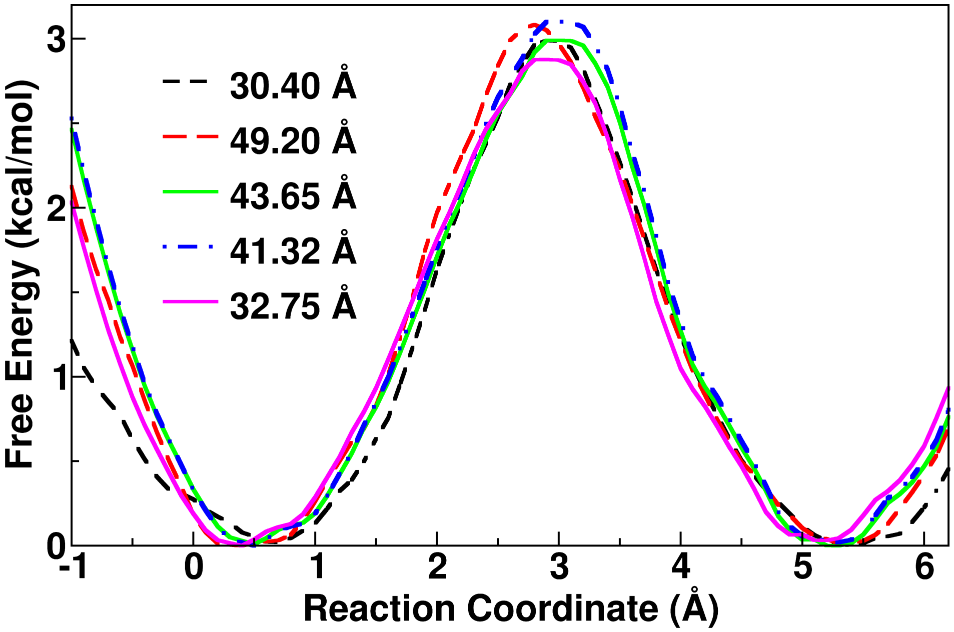

Figure S3: Free energy profiles for the motion of cation obtained using different initial configurations. The distances mentioned in the legend correspond to that between the cation-anion vacancies in each initial configuration.

Radial Distribution Functions: Structural correlations were characterized through radial distribution dunctions (RDFs).

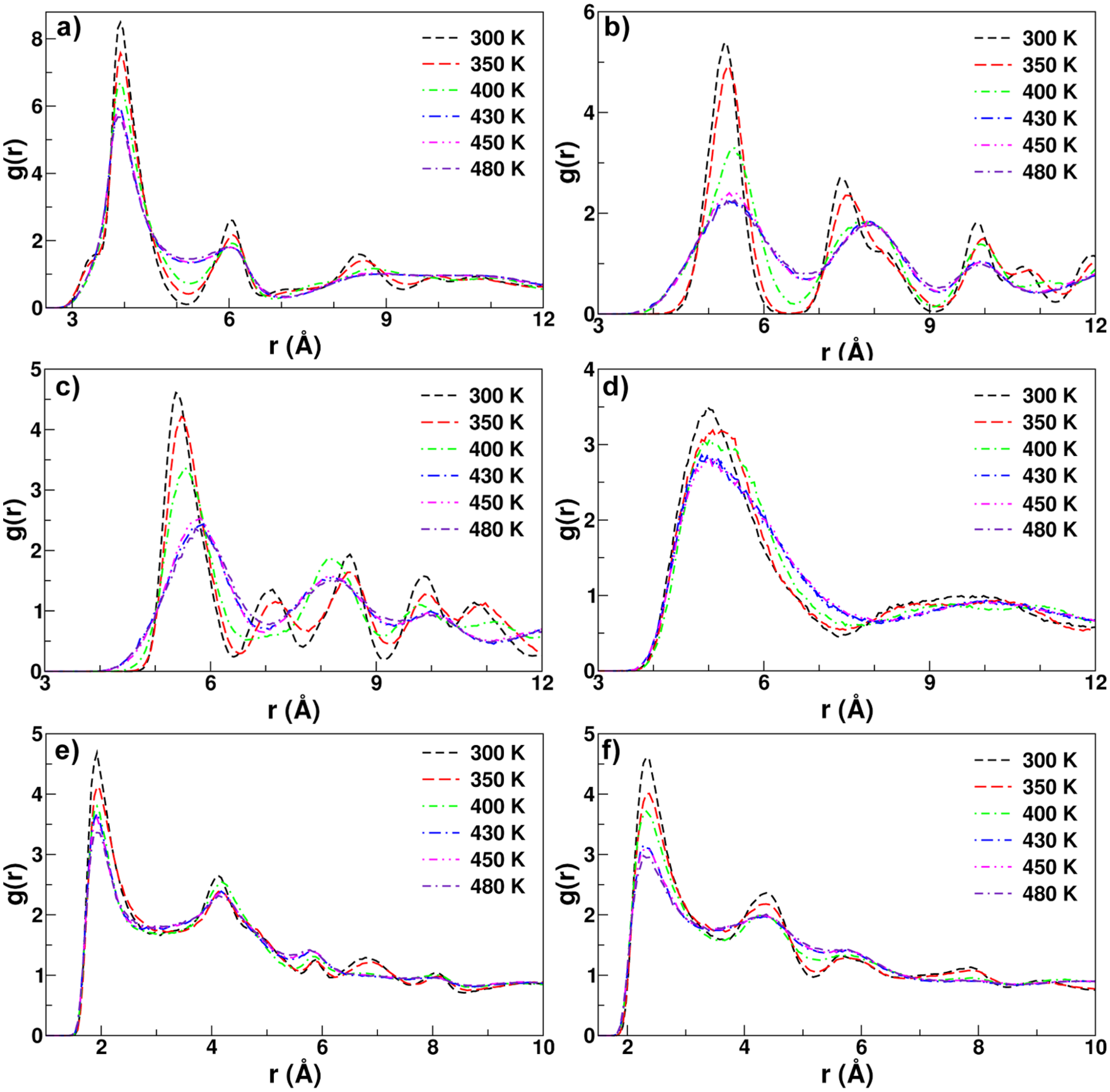

Figure S4: RDFs for a) cation–anion, b) cation–cation, c) anion–anion, d) tail-tail, e) H_N-O, and f) H_C-O pairs at various temperatures.

Cation–anion, cation–cation, anion–anion, and tail-tail (for perfluoro butyl) RDFs at different temperature are shown in **Figure** S4(a-d) respectively. The peak profiles broaden and shift to right with increase in temperature, as expected. The presence of strong N–H$\cdots$O hydrogen bonding interaction and weak C–H$\cdots$O hydrogen bonding interactions between triazolium ring of cation and sulfonate group of anion are seen from H_N–O and H_C–O RDFs respectively as shown in **Figure** S4(e and f). The effect of temperature is insignificant on H_N–O and H_C–O RDFs.

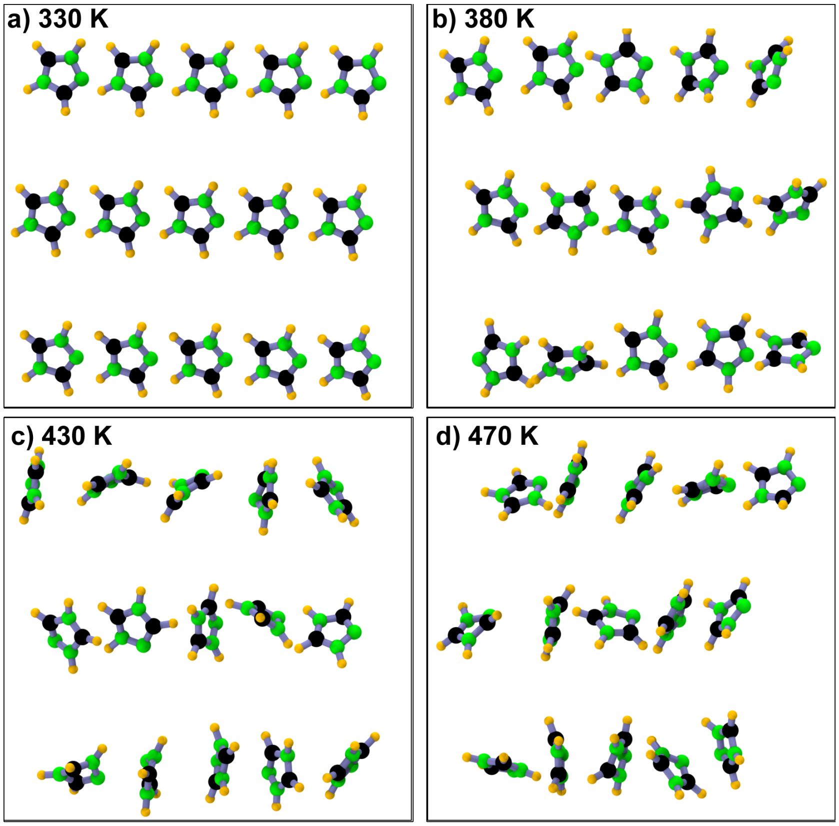

Figure S5: Snapshots of 1,2,4-triazolium rings from MD simulation of the perfect crystal depicts ring plane rotational order & disorder at a) 330 K, b) 380 K, c) 430 K, and d) 470 K. [carbon-black, nitrogen-green, hydrogen-orange (CPK)]

The variation of volume with temperature is shown in **Figure** S6 and is compared against the dimensional change of [TAZ][pfBu] obtained from experiment[S3] for different thermal phases.

The powder x-ray diffraction (PXRD) from MD simulations was calculated using mercury[S6] software at 300 K and 433 K and compared with the “simulated” PXRD pattern obtained from the experimental CIF file at 300 K (see **Figure** S7). The PXRD pattern calculated from MD simulation at 300 K closely resembles the experimental data.[S3] At higher temperature (433 K), several changes in the pattern are observed which could be useful when high temperature X-ray diffraction experiments are conducted, in future.

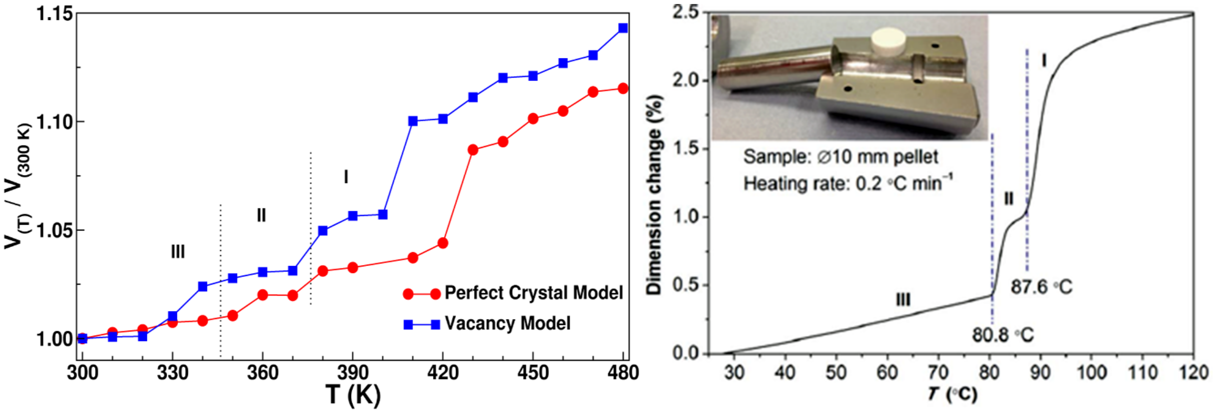

Figure S6: Left: Variation in the volume of simulation cell with temperature; Right: Temperature dependence of height change of a cylindrical dense pellet while heating from room temperature to 120 °C [Adapted from the work of Luo et al.[S3] copyright 2015 Royal Society of Chemistry].

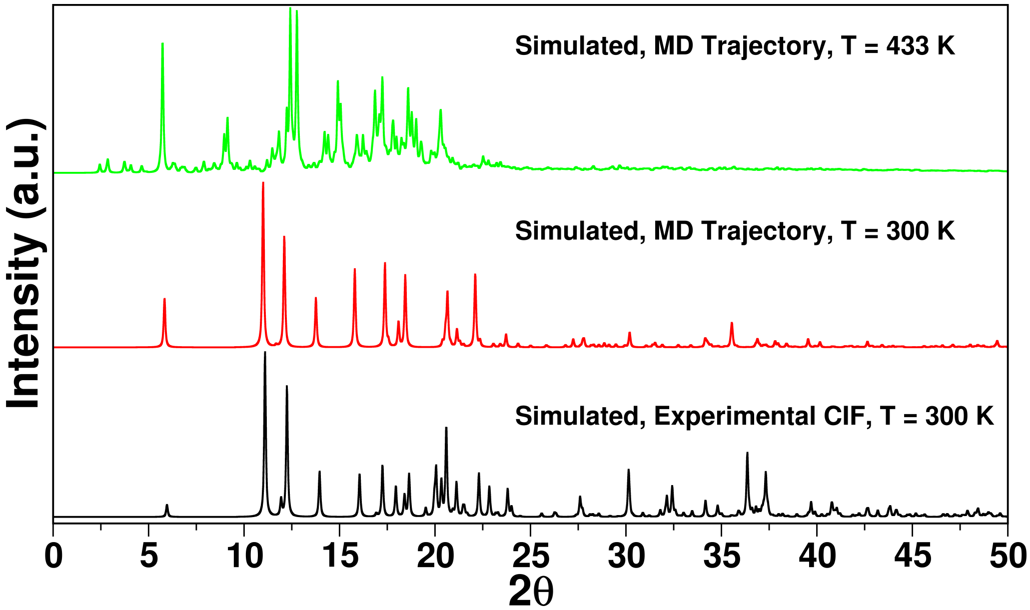

Figure S7: Comparison of the simulated powder XRD patterns obtained from experimental CIF and MD trajectory at different temperatures.

Vibrational density of states: Vibrational density of states (VDOS) at different temperature was calculated using the MD trajectory as the Fourier transform of the time autocorrelation functions of the atomic velocities (VACF), which can be written as

$$I(\omega) = \frac{1}{k_B T} \sum_j m_j \left[\frac{1}{2\pi} \int_{-\infty}^{\infty} exp(-i\omega t) \langle \mathbf{v}_j(0).\mathbf{v}_j(t) \rangle dt \right] \tag{1}$$

where $\mathbf{v}_j(t)$ is the velocity of atom type j at time t. Vibrational modes below 100 cm^{-1} show a red shift (softening) with an increase in temperature (**Figure** S8). Normal mode analyses show that the modes present below 100 cm^{-1} can be assigned to cation ring librational motions (by visualizing the atomic displacements/eigenvectors of such modes). The librational motions soften much closer to the transition point.

Normal-mode analysis: A separate trajectory was generated from classical molecular dynamics simulations of [TAZ][pfBu] POIPC at different temperatures. A number of configurations (one hundred) were selected from this trajectory and were energy minimized using the conjugate gradient method in LAMMPS.[S7] At each of these one hundred quenched configurations, the Hessian matrix of potential energy with respect to atomic coordinates was obtained and diagonalized using a normal-mode analysis program developed in our group.[S8] The resulting eigenvalues of the Hessian provide information on frequencies, whereas the atomic displacements of modes were assigned based on the eigenvectors of the Hessian. Atomic displacements were visualized in Jmol.[S9]

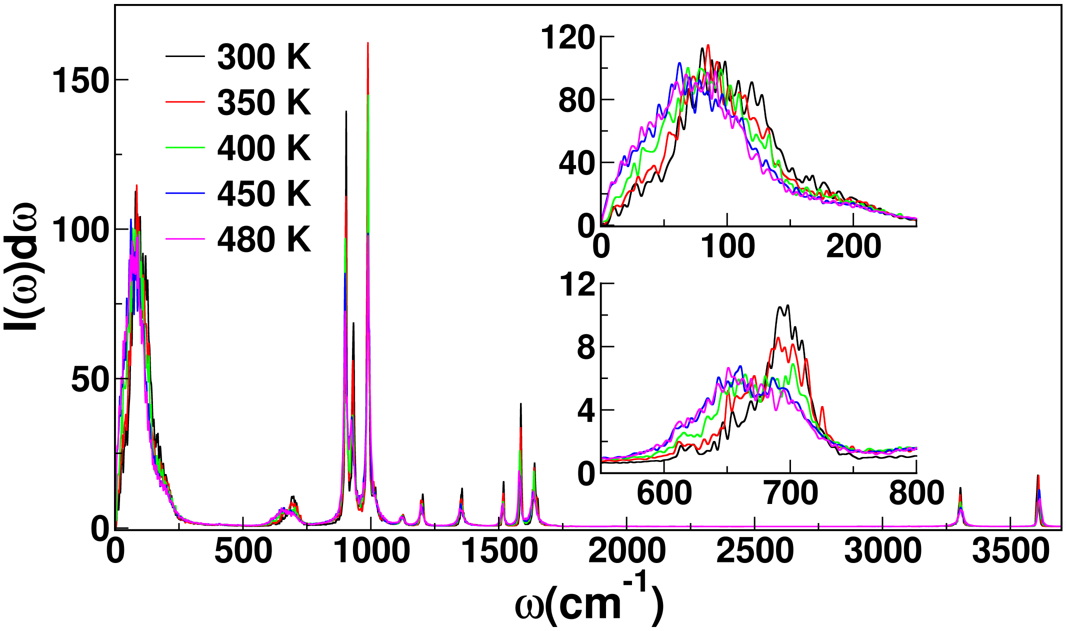

Figure S8: Vibrational density of states (VDOS) calculated for [TAZ][pfBu] from the power spectrum of the velocity autocorrelation function at different temperature (inset shows region of spectrum (a) below 150 cm^{-1}, and (b) between 600-750 cm^{-1}).

H-bond time correlation function: We have characterized the lifetime of the hydrogen bonds between acidic proton ($\mathrm{H_N}$) and anion oxygen atom in terms of two time correlation functions $\mathrm{S_{HB}}(t)$ and $\mathrm{C_{HB}}(t)$.[S10,S11] The relaxation of H-bond lifetime was studied by $\mathrm{S_{HB}}(t)$,

$$S_{HB}(t) = \frac{\langle h(0)H(t)\rangle}{\langle h\rangle} \tag{2}$$

where $h(t)$ is unity when a particular $\mathrm{H_N}$ atom and an anion oxygen atom is hydrogen bonded at time t, and zero, otherwise. On the other hand, $H(t) = 1$ if the tagged pair of atoms remain continuously H-bonded till time t, else zero. The structural relaxation of H-bonds was analysed by $\mathrm{C_{HB}}(t)$,

$$C_{HB}(t) = \frac{\langle h(0)h(t)\rangle}{\langle h\rangle} \tag{3}$$

where $\mathrm{C_{HB}}(t)$ exhibits a much slower decay than $\mathrm{S_{HB}}(t)$, as the former allows the possible breaking and reformation of H-bonds between the tagged pair of atoms. The geometric definition of H-bonding (distance, angle conditions) was the same as used in previous report[S10] and are provided below for the sake of completeness. A donor-acceptor (DA) pair is said to be hydrogen bonded, if the D-A distance is less than 3.5 Å, the H$\cdots$O distance less than 2.5 Å and the D-H$\cdots$O angle is greater than 140^o. The time resolutions used to obtain the $\mathrm{S_{HB}}(t)$ and $\mathrm{C_{HB}}(t)$ functions were 2.5 fs and 1 ps, respectively.

We fit the $\mathrm{S_{HB}}(t)$ function with a tri-exponential form,

$$S_{\mathrm{HB}}(t) = \sum_{i=1}^{3} a_i e^{-t/\tau_i} \tag{4}$$

whereas, a bimodal exponential decay and a constant term was used to fit the $\mathrm{C_{HB}}(t)$ function

$$C_{\mathrm{HB}}(t) = a_0 + \sum_{i=1}^{2} a_i e^{-t/\tau_i} \tag{5}$$

where the constant a_0 is included to take into account the non-zero asymptotic value of $\mathrm{C_{HB}}(t)$

at lower temperatures.

Table S3: Tri-exponential fit parameters for N-H$\cdots$O hydrogen bond lifetime correlation function (S$_{\mathrm{HB}}(t)$) at various temperature.

Temp. (K)	a$_1$	$\tau_1 (ps)$	a$_2$	τ_2 (ps)	a$_2$	τ_3 (ps)	$\langle\tau_S^{HB}\rangle$ (ps)
300	0.59	0.09	0.20	0.01	0.21	0.32	0.1223
350	0.63	0.10	0.18	0.01	0.19	0.30	0.1218
380	0.59	0.09	0.18	0.01	0.23	0.26	0.1147
390	0.60	0.08	0.19	0.01	0.21	0.28	0.1087
400	0.57	0.09	0.19	0.01	0.24	0.23	0.1084
420	0.63	0.09	0.20	0.01	0.17	0.25	0.1012
430	0.61	0.08	0.21	0.01	0.18	0.25	0.0959
440	0.55	0.08	0.22	0.01	0.20	0.20	0.0862
450	0.55	0.07	0.23	0.01	0.22	0.18	0.0804

Table S4: Bi-exponential fit parameters for N-H$\cdots$O hydrogen bond structural relaxations (C$_{\mathrm{HB}}(t)$) at various temperature.

Temp. (K)	a$_0$	a$_1$	$\tau_1 (ps)$	a$_2$	τ_2 (ps)
400	0.60	0.39	0.12	0.24	2.56
420	0.55	0.39	0.08	0.21	1.98
430	0.49	0.34	0.07	0.19	1.36
440	0.39	0.19	0.05	0.17	0.16
450	0.23	0.17	0.04	0.10	0.11

Dynamics in [TAZ][pfBu]: The mean distance traveled by a tagged particle can be estimated by calculating the Mean Square Displacement (MSD). The MSD for cation and anion are shown in **Figure** S9. The nature of displacement can be further investigated using the self-part of van Hove correlation function,[S12,S13] which can be written as

$$G_s(r,t) = \frac{1}{N}\sum_{i=1}^{N}\langle\delta(\mathbf{r} - \mathbf{r}_i(t) - \mathbf{r}_i(0))\rangle \tag{6}$$

where $\mathbf{r}_i(t)$ is time-dependent position of a particle and $4\pi r^2 G_s(r,t)$ is the probability of a tagged particle for a displaced distance r at time t.

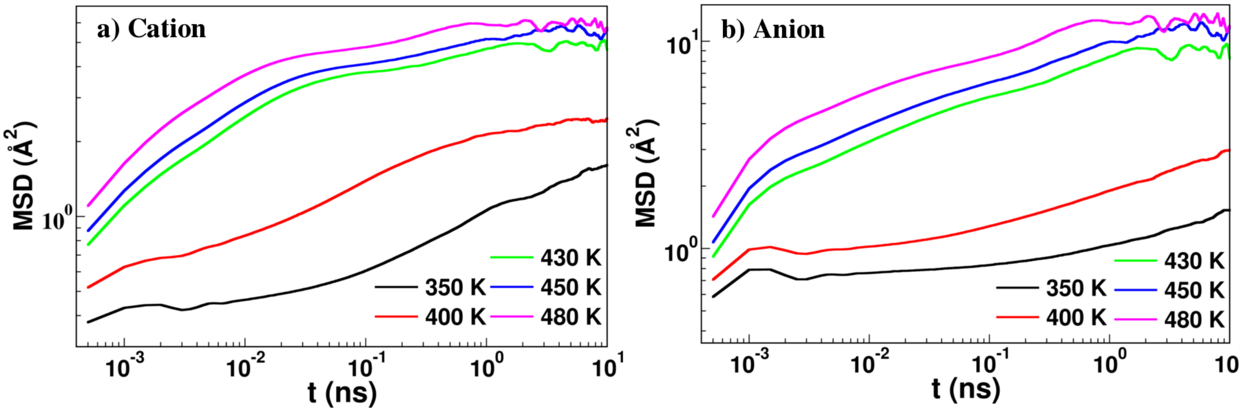

Figure S9: MSD of cations and anions calculated from MD simulations at various temperature.

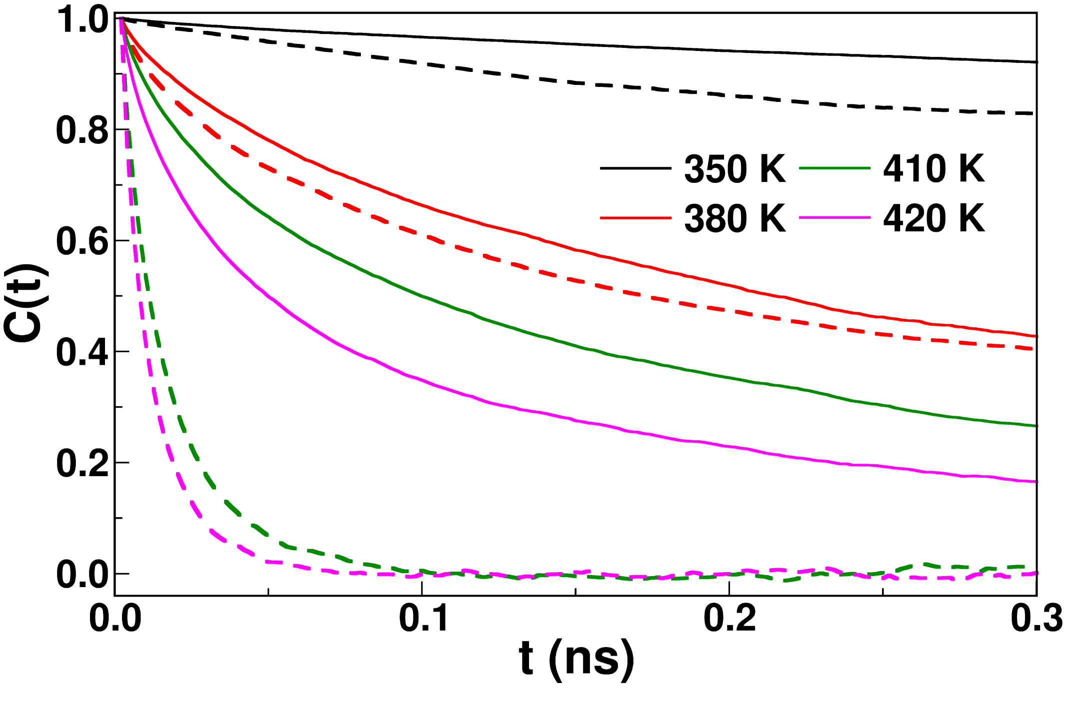

Figure S10: Auto time correlation function of ring plane normal of the cation at different temperatures: solid line - perfect crystal and dashed line - vacancy model. Data for the perfect crystal was also presented in **Fig.** 4 of main text.

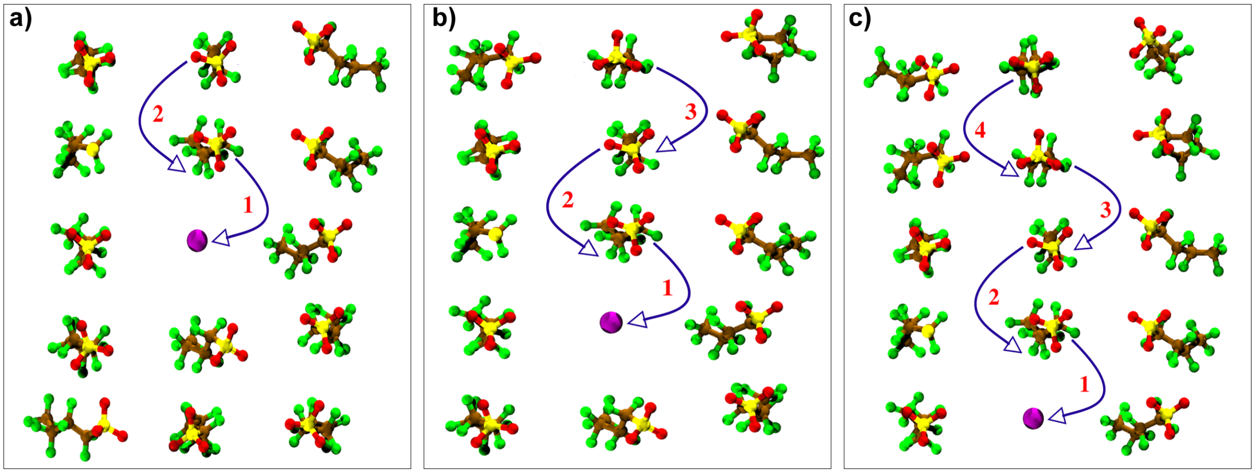

Figure S11: Snapshots (a-c) depict concerted hopping of anion in crystal simulation using the vacancy model [color scheme (CPK): carbon-ochre, oxygen-red, fluorine-green, sulfer-yellow and vacancy site-pink].

The ion hopping frequency Γ can be estimated within the framework of transition state theory (TST)[S14,S15]

$$\Gamma = \nu\, exp\left(\frac{-E_A}{k_B T}\right), \tag{7}$$

where ν is the attempt frequency and is typically assumed to be 10^{13} Hz.[S14–S16] The resulting hopping frequency using Eq. 7 for cations and anions are 8×10^{11} Hz and 2×10^{10} Hz respectively. However, the number of hopping events in the MD simulations at 500 K over a duration of 1 ns were observed to be seven and two for cations and anions respectively, which corresponds to jump frequencies of just 7×10^{9} and 2×10^{9} Hz. Thus, the hopping frequency in the vacancy based simulations are one to two orders of magnitude lesser than those obtained from the TST expression Eq. 7. The reason for the difference is not far to seek; it can likely be accounted by barrier recrossing, a well established phenomenon which reduces the attempt frequency ν in Eq. 7.

The jump diffusion coefficient (D_j) corresponding to an ion hopping to neighboring vacant site can be calculated as,[S16]

$$D_j = \lambda^2\Gamma/6, \tag{8}$$

where λ is a mean hopping distance.[S16] The calculated jump diffusion coefficients (using Γ values obtained from Eq. 7) for cations and anions are 5.7×10^{-4} cm^2 s^{-1} and 2.3×10^{-5} cm^2 s^{-1} respectively. These are about two orders of magnitude larger than diffusion coefficients obtained from the MSD. The difference is expected as Γ via TST itself is overestimated, as discussed earlier.

References

(S1) Manz, T. A.; Sholl, D. S. Chemically Meaningful Atomic Charges That Reproduce the Electrostatic Potential in Periodic and Nonperiodic Materials. *J. Chem. Theory Comput.* **2010**, *6*, 2455–2468.

(S2) Manz, T. A.; Sholl, D. S. Improved Atoms-in-Molecule Charge Partitioning Functional for Simultaneously Reproducing the Electrostatic Potential and Chemical States in Periodic and Nonperiodic Materials. *J. Chem. Theory Comput.* **2012**, *8*, 2844–2867.

(S3) Luo, J.; Jensen, A. H.; Brooks, N. R.; Sniekers, J.; Knipper, M.; Aili, D.; Li, Q.; Vanroy, B.; Wubbenhorst, M.; Yan, F.; Van Meervelt, L.; Shao, Z.; Fang, J.; Luo, Z.-H.; De Vos, D. E.; Binnemans, K.; Fransaer, J. 1,2,4-Triazolium perfluorobutanesulfonate as an Archetypal Pure Protic Organic Ionic Plastic Crystal Electrolyte for All-solid-state Fuel Cells. *Energy Environ. Sci.* **2015**, *8*, 1276–1291.

(S4) Hutter, J.; Iannuzzi, M.; Schiffmann, F.; VandeVondele, J. CP2K: Atomistic Simulations of Condensed Matter Systems. *Wiley Interdiscip. Rev. Comput. Mol. Sci.* **2014**, *4*, 15–25.

(S5) Mondal, A.; Balasubramanian, S. Quantitative Prediction of Physical Properties of Imidazolium Based Room Temperature Ionic Liquids through Determination of Condensed Phase Site Charges: A Refined Force Field. *J. Phys. Chem. B* **2014**, *118*, 3409–3422.

(S6) Macrae, C. F.; Edgington, P. R.; McCabe, P.; Pidcock, E.; Shields, G. P.; Taylor, R.; Towler, M.; van de Streek, J. *Mercury*: Visualization and Analysis of Crystal Structures. *J. Appl. Crystallogr.* **2006**, *39*, 453–457.

(S7) Plimpton, S. Fast Parallel Algorithms for Short-Range Molecular Dynamics. *J. Comput. Phys.* **1995**, *117*, 1–19.

(S8) Krishnan, M.; Balasubramanian, S. Vibrational Dynamics of Solid Poly(ethylene oxide). *Phys. Rev. B* **2003**, *68*, 064304.

(S9) Jmol: an open-source Java viewer for chemical structures in 3D. http://www.jmol.org/.

(S10) Chandra, A. Effects of Ion Atmosphere on Hydrogen-Bond Dynamics in Aqueous Electrolyte Solutions. *Phys. Rev. Lett.* **2000**, *85*, 768–771.

(S11) Balasubramanian, S.; Pal, S.; Bagchi, B. Hydrogen-Bond Dynamics near a Micellar Surface: Origin of the Universal Slow Relaxation at Complex Aqueous Interfaces. *Phys. Rev. Lett.* **2002**, *89*, 115505.

(S12) Del Pópolo, M. G.; Voth, G. A. On the Structure and Dynamics of Ionic Liquids. *J. Phys. Chem. B* **2004**, *108*, 1744–1752.

(S13) Jiang, W.; Yan, T.; Wang, Y.; Voth, G. A. Molecular Dynamics Simulation of the Energetic Room-Temperature Ionic Liquid, 1-Hydroxyethyl-4-amino-1,2,4-triazolium Nitrate (HEATN). *J. Phys. Chem. B* **2008**, *112*, 3121–3131.

(S14) Garcia-Belmonte, G.; Bisquert, J. Entropy factor in the hopping frequency for ionic conduction in oxide glasses induced by energetic clustering. *J. Chem. Phys.* **2005**, *123*, 074504.

(S15) Van der Ven, A.; Ceder, G.; Asta, M.; Tepesch, P. D. First-principles theory of ionic diffusion with nondilute carriers. *Phys. Rev. B* **2001**, *64*, 184307.

(S16) Garcia-Belmonte, G.; nadas, J. G.-C.; Bisquert, J.; Person, C. Jump Diffusion Coefficient of Different Cations Intercalated into Amorphous {WO3}. *Solid State Ionics* **2006**, *177*, 1635–1637, Solid State Ionics 15: Proceedings of the 15th International Conference on Solid State Ionics, Part I.